Nano Energy (2013) 2, 1225–1231

Available online at www.sciencedirect.com

ScienceDirect

journal homepage: www.elsevier.com/locate/nanoenergy

RAPID COMMUNICATION

Mapping of strain-piezopotential relationship along bent zinc oxide microwires

Dalong Geng[a], Alex Pook[b], Xudong Wang[a,*]

[a]Department of Materials Science and Engineering, University of Wisconsin-Madison, 1509 University Ave., Madison, WI 53706, USA
[b]Department of Engineering Physics, University of Wisconsin-Madison, Madison, WI 53706, USA

Received 13 April 2013; accepted 17 May 2013
Available online 28 May 2013

KEYWORDS
Piezoelectric;
Potential mapping;
ZnO microwire;
3DKPM;
Screening effect

Abstract
Piezoelectric nanowire based nanogenerator is a promising technology to harvest ambient mechanical energy. It is essential to experimentally quantify the strain-piezopotential relationship on nanowires for the development of high-output nanogenerators. In this paper, 3D Kelvin probe microscopy (3DKPM) is applied to precisely mapping the piezopotential along a bent ZnO microwire (MW). In order to remove the charge screening effect and recover the actual piezopotential generated by the MW, an external DC bias was applied along the axial direction of the bent MW. This external field drove charged species in and outside of the MW to the two oppositely-biased ends, respectively, and thus minimized the screening effect. We also developed a numerical method to calculate the strain distribution along the bent ZnO MW based on its scanning electron microscopy (SEM) image, with which the strain-piezopotential relationship was obtained. The overall theoretical and experimental relationships showed a good match, indicating 3DKPM under biased condition can be an effective approach for quantifying piezopotential from strained nanomaterials. The detected piezopotential is independent of screening charge and external screening effect, and is not affected by the sharp topography variation along the edge of wires. It could serve as an important methodology for revealing nanoscale piezoelectric and flexoelectric properties.

Introduction

Recently, piezoelectric nanowire (NW)-based nanogenerator has been attracting much attention as a promising technology for nanoscale ambient mechanical energy harvesting [1–6]. Nanogenerators have the potential to become a practical power source for charging batteries, powering small electronics, and even implantable biomedical devices [7–15]. Owing to the advanced nanofabrication techniques and good material property control, the output of NW-based nanogenerators is experiencing a rapid improvement, which increased from the original sub-nanowatt level to almost milliwatt currently [16]. Many nanogenerator-powered small electronic devices have demonstrated normal functions, such as pH sensors [16], light

*Corresponding author. Tel.: +1 608 890 2667.
E-mail address: xudong@engr.wisc.edu (X. Wang).

2211-2855/$ - see front matter © 2013 Elsevier Ltd. All rights reserved.
http://dx.doi.org/10.1016/j.nanoen.2013.05.008

emitting diodes [17], liquid crystal displayers [18], and so forth. The operation principle of NW-based nanogenerators lies on the deflection of NWs and therein strain-induced piezoelectric potential, or piezopotential. Aside from the rapid engineering development, fundamental understanding of nanogenerator output capability and efficiency is lagged behind. A few numerical calculations revealed the strain-piezopotential relationship in insulating and semiconducting ZnO NWs; [19,20] whereas the measured outputs still exhibit big discrepancies from the calculations. An exciting phenomenon was proposed that a nanoscale strain gradient can significantly enhance the piezoelectric response, i.e. the flexoelectric effect, which is expected to boost the nanogenerator's output by a few hundred percent when NW's size is within tens of nanometers [21]. However, such enhancements have only been shown theoretically. In order to prove the exciting theories and provide a reliable guideline for nanogenerator development, it is essential to experimentally quantify the strain-piezopotential relationship on NWs.

Nevertheless, characterizing piezopotential along a NW possesses a great challenge. Quantifying piezopotential differences across the small diameter of a NW requires high precision and resolution in terms of both location and potential measurements. Atomic force microscopy (AFM)-based characterization methods would ideally satisfy such requirements. The first demonstration of nanoscale piezopotential was done by current-AFM (c-AFM), but only limited to the NW's tip position [4]. Establishing the relationship between piezopotential and strain distribution along the entire NW body, as predicted by calculation, requires more sophisticated measurement and data processing. Raster scanning a deflected NW suffers from huge artifacts due to surface topography contribution [22]. Recently, our group developed a new Kelvin probe microscopy (KPM) approach that can effectively eliminate the topographic artifacts from NW's side walls and maps the potential distribution around NW's cross-section. It is thus named 3DKPM. 3DKPM can precisely quantify the potential difference between two opposite surfaces of a deflected NW with nanometer-level resolution [23]. It is therefore promising for determining the nanoscale strain-piezopotential relationship. However, 3DKPM is a very slow process. Piezopotential on NWs can be quickly screened in atmosphere and leaves the measurement in vain. To address this challenge, we preliminarily demonstrated that applying an external bias could offset the screening effect and make the slow 3DKPM measurement possible. In this paper, we systematically investigated the effect of external biases. Under the optimal external bias, the potential distribution in the 3D space along a bent ZnO microwire (MW) body was successfully constructed. The potential distribution exhibited a good match with theoretical calculation.

Material and methods

Fig. 1a schematically shows the experimental setup for 3DKPM mapping piezopotential. A pair of wedge-shape gold electrodes was fabricated on a Si substrate covered with a

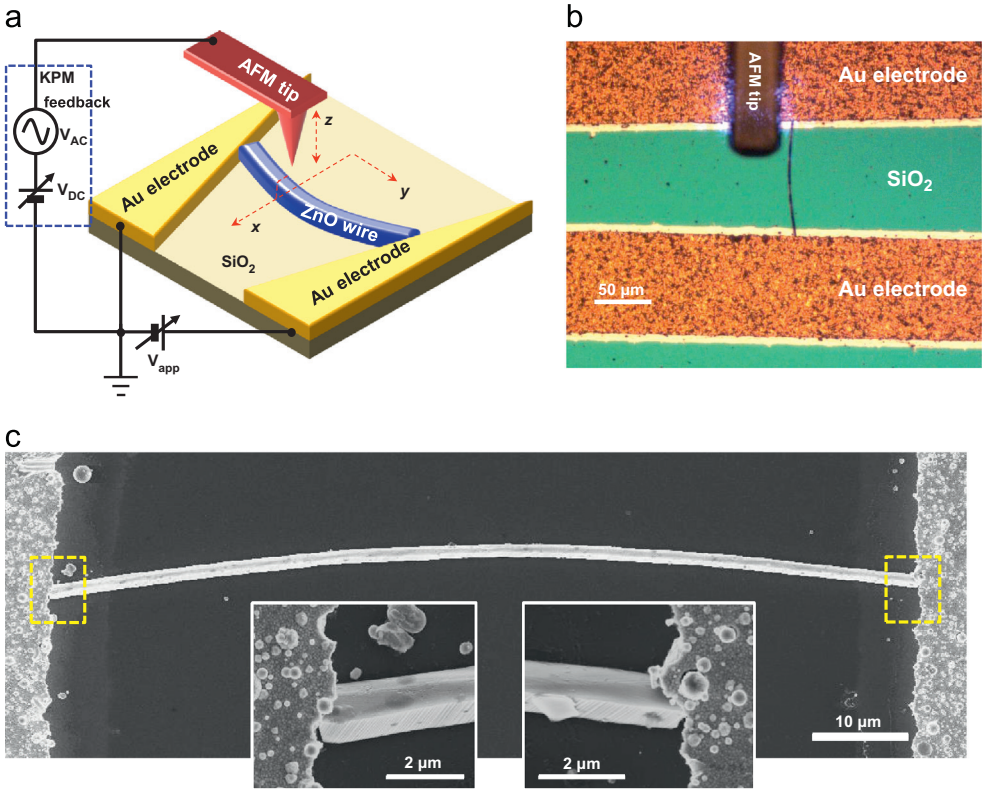

Fig. 1 Experiment setup of 3DKPM measurement on a bent ZnO MW. (a) Schematic experimental design of 3DKPM for measuring piezopotential difference on a bent ZnO MW. (b) Optical image of the bent ZnO MW inside the wedge-shaped gold trench that is ready for 3DKPM characterization. (c) SEM image of the bent ZnO MW inside the trench. Insets are enlarged image of two contact areas showing the MW is tightly clapped by the rough edges of the gold electrodes.

layer of insulating SiO_2. A ZnO MW was bent and immobilized in the trench manipulated by AFM probe. An external DC bias was applied between the gold electrodes to generate an electric field along the *y* axis direction. 3DKPM mapping was conducted using a conductive AFM tip scanning along the *x* axis direction. The 3DKPM operation details have been reported in our previous publication [23]. A spatial electric potential map was constructed on the *x*–*z* plane after each 3DKPM scan. A series of *y* positions were selected along the bent ZnO MW for mapping the strain–piezopotential relationship. Fig. 1b is an optical microscopic image of the wedge-shaped gold trench with a bent ZnO MW held inside and positioned for 3DKPM scanning. In order to minimize the electrostatic influence to KPM measurement, the Au electrode under the AFM cantilever was grounded and the opposite side was biased. Although bending of such a large ceramic ZnO wire creates significant strain energy, the rough edges gold electrodes can tightly clap both ends of the MW and keep it flat on the substrate trench surface (Fig. 1c and insets). This feature is critical for obtaining reliable 3DKPM data across the MW's cross-sections. It is also an important prerequisite for our assumption of uniform external electrical field along the wire body.

Conductive AFM probe sensitivity symmetry was confirmed prior to performing 3DKPM characterization by measuring the spatial potential distribution before and after rotating the sample 180 degrees along the *z*-axis. Identical potential distributions confirmed that both sides of the conductive AFM tip were equally sensitive to electric potential when raster scanning laterally. This sensitivity symmetry is necessary for precisely mapping the piezoelectric potential around the MWs.

Six positions were selected along the bent ZnO MW for 3DKPM mapping. The scan directions of 3DKPM were perpendicular to the *c* axis of the ZnO MW. Because of the bent configuration, the scan direction was slightly deviated from the normal direction of the external electric field, which gave rise to asymmetric electric potential background in 3DKPM mapping. This potential background was removed from 3DKPM raw data by subtracting the base potential, which was assumed to change linearly along the *x* direction (scanning direction). The piezopotential was determined by calculating the potential difference between the two sides of the bent ZnO MW in a 3DKPM potential map (see details in Ref. [23]).

The strain distribution along the bent MW was obtained by fitting a polynomial curve to an SEM image of the bent ZnO MW and substituting this polynomial into the general strain–stress formula (details are included in supplementary materials SI). Based on the strain information, the theoretical piezoelectric potential across ZnO MW was calculated following the method presented in our previous publication [24].

Results and discussion

The topographic image of the bent ZnO MW was characterized first using AFM to obtain the shape information of the MW and define the position of 3DKPM scan (Fig. 2a). The uniform contrast along the MW's body also evidences the flat positioning of the bent MW. The six 3DKPM scan positions are marked by green arrows in the image. At each selected

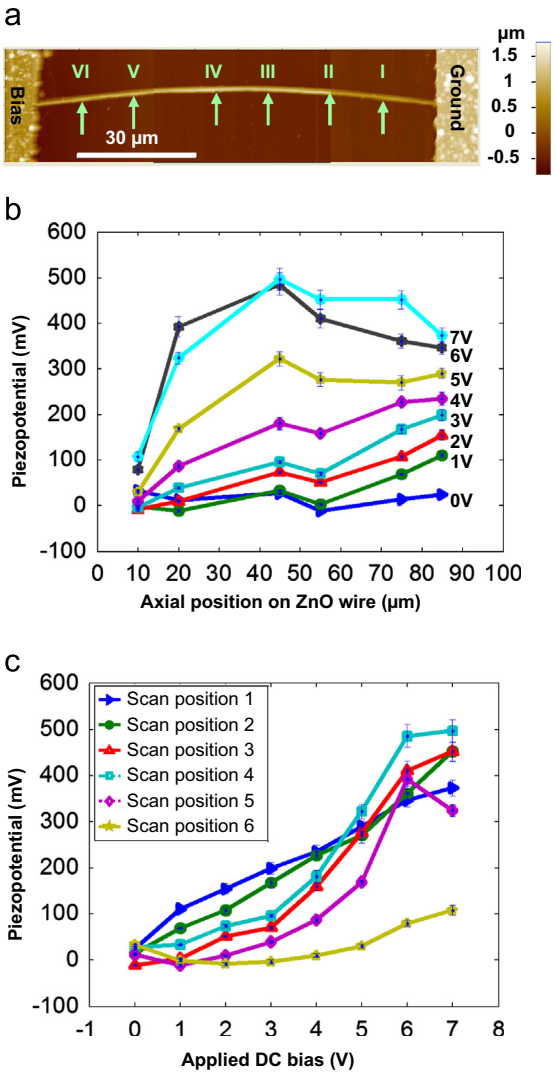

Fig. 2 Measurement results of the piezopotential difference along a bent ZnO MW. (a) An AFM topography image showing the flat position of the MW on trench surface. The six 3DKPM scanning positions are marked by green arrows. (b) Piezopotential difference measured by 3DKPM at the six scanning positions under DC bias from 0 V to 7 V. (c) Plot of the piezopotential difference change as a function of applied DC bias. (For interpretation of the references to color in this figure legend, the reader is referred to the web version of this article.)

position, 3DKPM was performed to map the electric field distribution around the wire surface (A typical 3DKPM image is included in the supplementary materials, SII, Fig. S4). From the 3DKPM potential maps at all six positions, the potential differences across the wire's diameter were obtained as a function of position (blue triangles in Fig. 2b). It is obvious that the obtained potential differences are within the noise level and no relationship with the position (or strain) can be identified. The diminish of detectable piezoelectric potential under zero bias is believe to be due to internal screening effect from free charge carriers and external screening from charged species from atmosphere.

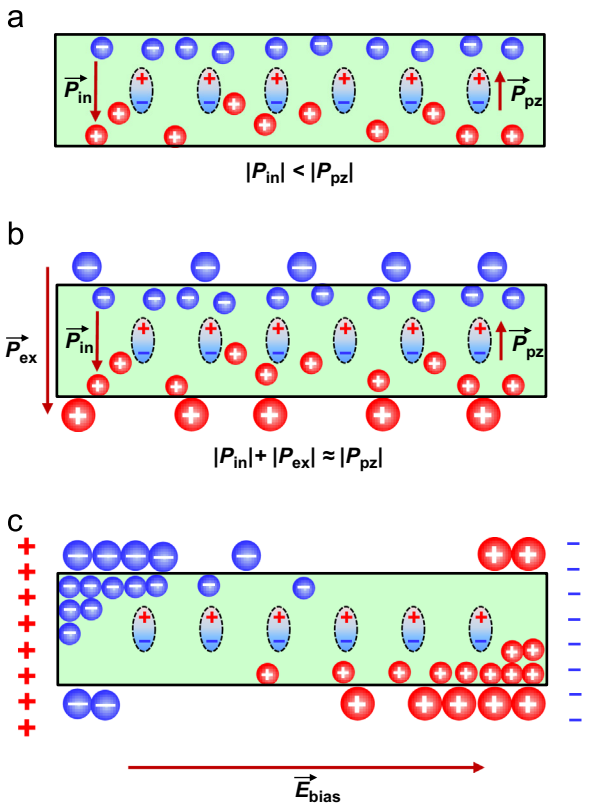

Fig. 3 Schematic of the charge screening and uncovering mechanisms. (a) Internal screening effect in a strained ZnO wire. The intrinsic piezoelectric polarization is P_{pz} upon the appearing of strain. The induced redistribution of free carriers inside ZnO wire creates a counter polarization P_{in} and screens P_{pz}. This screening occurs immediately when P_{pz} appears. The detectable piezopotential is determined by the difference between the absolute values of P_{in} and P_{pz}, (b) Equilibrium state when both internal and external screening occurs. The external screening effect is due to the adsorption of charged species from ambient air unto the wire surface. This adsorbed charged species contribute an addition polarization (P_{ex}) that further screens the P_{pz}. When equilibrium state is reached, the sum of internal and external screen equals to the P_{pz}. This is the complete screen, and no piezopotential can be detected. (c) Biased condition. When an external bias is applied along the axial direction of the wire, internal and external charges are attracted toward both ends following the electric field and expose the screened region (mostly at the center). From the charge depleted region, P_{pz} can be detected with desirable accuracy.

When a DC bias was applied between the two electrodes holding the bent ZnO MW, piezopotential differences emerged in 3DKPM characterizations. Fig. 2b plots the potential differences determined from 3DKPM maps as functions of MW's axial location under different external biases (V_b) from 0 V to 7 V. As V_b increased (1 V, green circles in Fig. 2b), the piezopotential difference first appeared near the grounding electrode side (position I and II), whilst the other points remained the same level as the non-biased values. The piezopotential difference at the center of wire (position III, VI, V) became distinguishable when V_b was raised above 2 V. The detectable piezopotential differences at all these points (positions I–V) increased following the increase of V_b. The three center points increased with a faster pace compared to the two end points (I and II) near the ground side and saturated around 400–500 mV when V_b reached 6–7 V. However, the piezopotential difference measured at the very end of the MW near the biased electrode remained at the noise level under V_b from 1 to 5 V and only slightly increased to ~100 mV when V_b was raised to 6–7 V. The piezopotential difference changes as function of V_b at different measuring locations are plotted in Fig. 2c, where the increasing trend and saturating feature can be clearly observed.

In order to determine the possible influence from applied bias, 3DKPM was conducted on a straight ZnO MW placed between the same electrode trench under different V_b (supplemental material, SIII, Fig. S5). No obvious potential differences were detected when V_b was varied from 0 V to 7 V. This experiment suggests that the contribution of V_b to potential difference measured by 3DKPM is negligible and the detected values from deflected MW can reflect the piezopotential evolution from the bent ZnO MW.

The evolution of detected piezopotential difference under different V_b can be understood by the screening model (Fig. 3). Ideally, piezoelectric polarization (P_{pz}) appears as soon as a strain is introduced to a piezoelectric material. As long as the strain remains, the P_{pz} is preserved under an open circuit condition (such as our bending case), and thus the piezopotential. For a semiconductor piezoelectric material, such as ZnO, finite amount of free charges can be quickly redistributed under the influence of P_{pz}, forming a counter polarization (P_{in}) internally (Fig. 3a). This is the internal screening effect. When $|P_{in}| < |P_{pz}|$, the internal screening is partially implemented and a certain amount of piezopotential is still detectable externally. In a more reality case, when a strained piezoelectric material is placed in atmosphere, charged species from atmosphere (P_{ex}) are likely attracted toward the charged surfaces of the piezoelectric material and further screen the P_{pz} (Fig. 3b). This phenomenon becomes more obvious under extended time or can be facilitated by external fields, which is the case of our 3DKPM characterization. Therefore, the bent ZnO MW system would reach the charge equilibrium quickly during 3DKPM measurement ($|P_{in}|+|P_{ex}| \approx |P_{pz}|$) and no piezopotential difference was detected initially.

When an external bias is applied along the MW's axial direction, both internal and external charges will be redistributed accordingly. Both negative internal charges and negatively charged surface species will move and accumulate at the positively biased end; whilst both positive internal charges and positively charged surface species will move and accumulate at the negative end (Fig. 3c) Their distribution can be controlled by many factors, such as effective mass, mobility, individual volume, electrostatic interaction, absorption energy, etc. and requires a complex model to quantify the distribution, which is beyond the scope of this paper. Qualitatively, as the internal and external charge is removed by the applied bias, the intrinsic P_{pz} becomes detectable. When V_b is low, the screening charges start to be pushed away from both ends. Due to the much higher mobility of electrons, the screening effect was initially broken on the negative side.

This situation is corresponding to the observed initial piezopotential emerging at positions I and II (see Fig. 2b and c). As V_b further increases, both negative and positive charges were gradually moved toward both sides passing the center region of the MW. Therefore, with less screening charges, higher piezopotential is detected. This is corresponding to the rapid increase of detected piezopotential in the center wire region (positions III, IV, and V) when V_b increases from 2 V to 5 V. When all the screening charges are depleted or the redistribution of charges reaches an equilibrium condition, the detectable piezopotential saturates (V_b=6–7 V for positions III, IV, and V).

As illustrated in Fig. 3c, due to the opposite moving directions of positive and negative charges, the screening charge in the center region of the MW is depleted most completely. This would be the reason of the rapid increase of detected piezopotential at positions III, IV, and V when V_b rises. When the saturation condition is reached, the detected piezopotential difference should be able to represent the intrinsic piezopotential from the bent ZnO MW. At the positively biased side, electrons and other negatively charged species accumulate around the wire body and fully screen all possible piezopotential (position VI). Therefore, nearly no change of the piezopotential difference was detected under a wide range of V_b. At the negatively biased side, positively charged species accumulates (positions I and II). However, due to the limited mobility of positive charges in n-type ZnO, the screening effect from the positive charges may be less effective compared to negative charges. Therefore, increase of detectable piezopotential difference still rises with increased V_b but with a slower rate compared to the center region. Nevertheless, because of the incomplete screening and non-saturation situation, the piezopotential differences detected from this side cannot fully reflect intrinsic piezopotential.

Based on above analysis and obtained 3DKPM potential distribution at different wire positions, the potential distribution around the bent ZnO MW can be constructed. As shown in Fig. 4a, the six 3DKPM potential maps were integrated with the bent ZnO wire body, providing a direct visualization of surface and space potential change as a result of straining. The potential maps were selected from 3DKPM measurement under V_b=7 V. From the picture, potential on the left (stretched) side of the bent ZnO NW is higher than that on the right (compressed) side, which is consistent with theoretical calculations [19,20,24,25].

In order to further test the accuracy of piezopotential measurement and our screening hypothesis, piezopotential difference was calculated as a function of strain. The strain distribution along the bent ZnO NW was extracted from its SEM

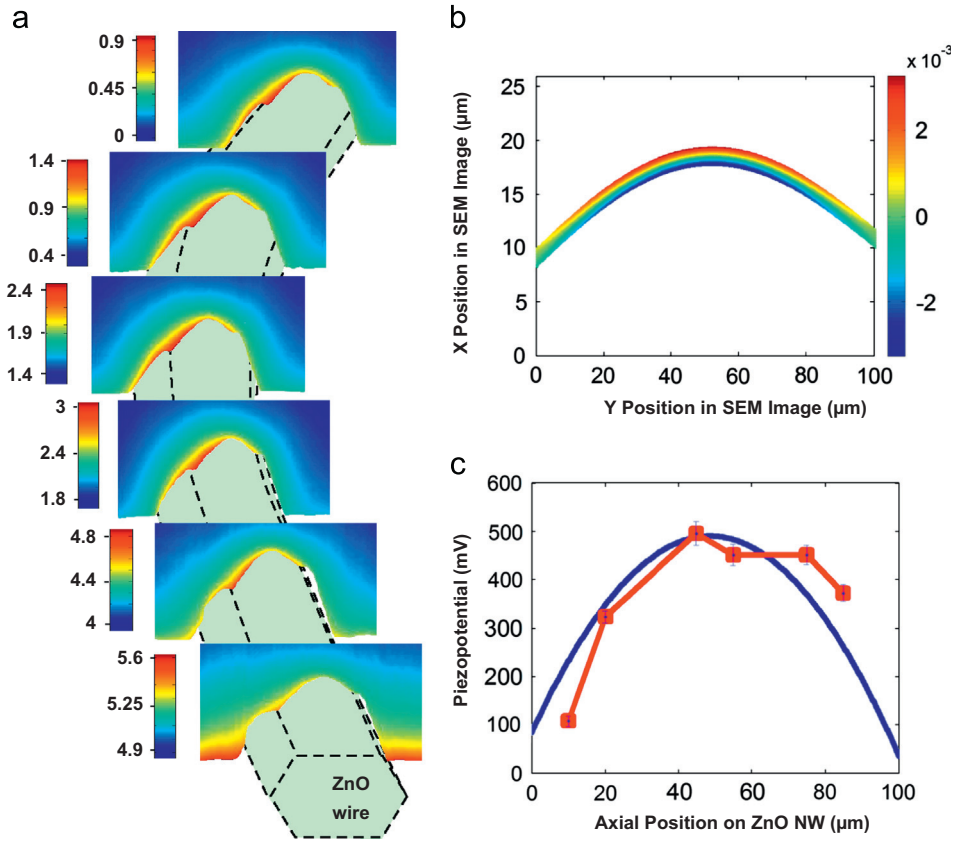

Fig. 4 Construction of piezopotential difference-strain relationship. (a) 3DKPM maps obtained at different positions along the bent ZnO MW under a DC bias of 7 V and constructed potential distribution along the MW. (b) Strain distribution on the bent ZnO MW calculated based on the SEM image. (c) Calculation (smooth blue line) and measurement (red squares) results of piezopotential difference based on the strain distribution calculated in (b). (For interpretation of the references to color in this figure legend, the reader is referred to the web version of this article.)

image (details included in the supplementary materials, SI). Fig. 4b shows the calculated strain distribution, where the maximum strain occurs at the center region of the bent ZnO MW and reduces to almost zero at the two contact end points. Based on the strain information, the piezopotential differences were calculated using the numerical model developed in our group earlier [24]. It should be noted that since the diameter of the bent ZnO wire is ~1.5 μm, the nanoscale flexoelectric effect was not considered in our calculation. Fig. 4c plots the calculated (smooth blue line) and measured (at V_b=7 V; red squares) piezopotential difference between the compressive and extension sides as a function of wire position. In both curves, piezopotential difference exhibits a maximum value at the center of the bent ZnO NW (496 mV from measurement and 490 mV from calculation) where the strain is the greatest and decreases toward both ends when strain drops. Comparing the piezopotential differences obtained from calculation and 3DKPM measurements, the center three points (III, IV, and V) exhibit an excellent match, whilst the three end points (I, II, and VI) are more deviated. This result is consistence with our charge screening hypothesis as discussed earlier. This result evidences the feasibility of 3DKPM technique for piezopotential characterization on bent wire surfaces.

Conclusions

In this paper, a 3DKPM method to map the strain-piezopotential relation on a bent wire structure is presented. The piezopotential is likely screened by internal charge carriers and charged species from atmosphere. This screening effect is fatal to the characterization of the real piezopotential independent of time and environment. To address this challenge, an external DC bias was applied along the axial direction of the bent MW. The external potential attracts charged species in and outside of the MW to oppositely-biased two ends, respectively, and thus minimizes the screening effect. Through this approach, piezopotential differences were obtained as a function of strain. The measurement results were compared to theoretical calculations, which showed a good match, indicating 3DKPM under biased condition can be an effective approach for quantifying piezopotential from strained nanomaterials. This is the first experimental demonstration of strain-piezopotential relationship on bent piezoelectric wires. The detected piezopotential is independent of screening charge and external screening effect, and is not affected by the sharp topography variation along the edge of wires. It could serve as an important methodology for revealing nanoscale piezoelectric and flexoelectric properties.

Acknowledgements

We thank Mr. Dylan Bayerl for the help with 3DKPM characterization and Dr. Chengliang Sun for preparing the trenched gold electrodes. This research is supported by NSF CMMI-1148919.

Appendix A. Supporting information

Supplementary data associated with this article can be found in the online version at http://dx.doi.org/10.1016/j.nanoen.2013.05.008.

References

[1] Y. Qin, X.D. Wang, Z.L. Wang, Nature 451 (7180) 809-U5.
[2] X.D. Wang, Y.F. Gao, Y.G. Wei, Z.L. Wang, Nano Research 2 (3) (2009) 177-182.
[3] X.D. Wang, J.H. Song, J. Liu, Z.L. Wang, Science 316 (5821) (2007) 102-105.
[4] Z.L. Wang, J.H. Song, Science 312 (5771) (2006) 242-246.
[5] X. Wang, Nano Energy 1 (1) (2012) 13-24.
[6] B. Kumar, S.-W. Kim, Nano Energy 1 (3) (2012) 342-355.
[7] A.P. Chandrakasan, N. Verma, D.C. Daly, Annual Review of Biomedical Engineering 10 (2008) 247-274.
[8] J.M. Donelan, Q. Li, V. Naing, J.A. Hoffer, D.J. Weber, A.D. Kuo, Science 319 (5864) (2008) 807-810.
[9] J. Granstrom, J. Feenstra, H.A. Sodano, K. Farinholt, Smart Materials and Structures 16 (5) (2007) 1810-1820.
[10] G.K. Ottman, H.F. Hofmann, A.C. Bhatt, G.A. Lesieutre, IEEE Transactions on Power Electronics 17 (5) (2002) 669-676.
[11] J.A. Paradiso, T. Starner, IEEE Pervasive Computing 4 (1) (2005) 18-27.
[12] S. Priya, Journal of Electroceramics 19 (1) (2007) 167-184.
[13] R. Yang, Y. Qin, C. Li, G. Zhu, Z.L. Wang, Nano Letters 9 (3) (2009) 1201-1205.
[14] H. Zhang, Y. Yang, T.-C. Hou, Y. Su, C. Hu, Z.L. Wang, Nano Energy, (2013).
[15] C. Xu, C. Pan, Y. Liu, Z. Wang, Nano Energy 1 (2) (2012) 259-272.
[16] S. Xu, Y. Qin, C. Xu, Y.G. Wei, R.S. Yang, Z.L. Wang, Nature Nanotechnology 5 (5) (2010) 366-373.
[17] L. Gu, N.Y. Cui, L. Cheng, Q. Xu, S. Bai, M.M. Yuan, W.W. Wu, J.M. Liu, Y. Zhao, F. Ma, Y. Qin, Z.L. Wang, Nano Letters 13 (1) (2013) 91-94.
[18] Y.F. Hu, Y. Zhang, C. Xu, G.A. Zhu, Z.L. Wang, Nano Letters 10 (12) (2010) 5025-5031.
[19] Y. Gao, Z.L. Wang, Nano Letters 7 (8) (2007) 2499-2505.
[20] Y. Gao, Z.L. Wang, Nano Letters 9 (3) (2009) 1103-1110.
[21] M.S. Majdoub, P. Sharma, T. Cagin, Physical Review B: Condensed Matter 77 (12) (2008).
[22] D.S.H. Charrier, M. Kemerink, B.E. Smalbrugge, T. de Vries, R.A.J. Janssen, Acs Nano. 2 (4) (2008) 622-626.
[23] D.J. Bayerl, X.D. Wang, Advanced Functional Materials 22 (3) (2012) 652-660.
[24] C.L. Sun, J.A. Shi, X.D. Wang, Journal of Applied Physics 108 (3) (2010).
[25] G. Mantini, Y.F. Gao, A. D'Amico, C. Falconi, Z.L. Wang, Nano Research 2 (8) (2009) 624-629.

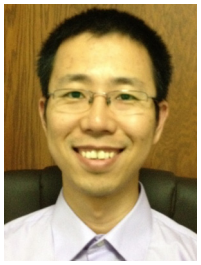

Dalong Geng is a graduate student in the department of Materials Science and Engineering at University of Wisconsin-Madison. He joined Professor Xudong Wang's group in 2011. His research interests include atomic force microscopy characterization and nanoscale piezoelectric property study. He currently has been focusing on quantification of strain gradient – piezoelectric potential relationship on strained piezoelectric and ferroelectric nanowires.

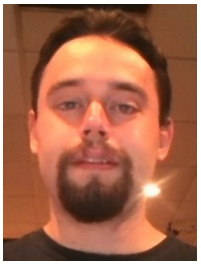

Alex Pook is an undergraduate student in the Engineering Physics Department at the University of Wisconsin-Madison. His areas of interest include MEMS design, fabrication and application of piezoelectric nanostructures, semiconductor electronics, and computer science. He is currently completing thesis work on geometric analysis of piezoelectric nanowires.

Xudong Wang is an assistant professor in the department of Materials Science and Engineering at University of Wisconsin–Madison. His research interests include studying the growth and assembly of oxide nanowire arrays, understanding the coupling effect of semiconductor properties and piezoelectric charge displacement, and developing nanogenerator that uses piezoelectric nanomaterials to convert low level mechanical energy into electricity. He is the recipient of NSF CAREER Award, DARPA Young Faculty Award, 3M Non-Tenured Faculty Award, Ross Coffin Purdy Award, Young Innovators Under 35 Award, and KAUST research fellow. He has published 62 papers in peer reviewed scientific journals, contributed 7 book chapters in his research field, and holds 5 patents/provisional patents on oxide nanostructures and nanomaterial-enhanced energy harvesting. His publications have been cited over 4000 times by peers and his current h-index is 30.